J Mater Sci (2012) 47:535–552
DOI 10.1007/s10853-011-5942-5

ANNIVERSARY REVIEW

Silicon nitride: the engineering material of the future

Zoran Krstic · Vladimir D. Krstic

Received: 23 June 2011 / Accepted: 8 September 2011 / Published online: 22 September 2011

Abstract The purpose of this review is to present the recent developments in silicon nitride (Si_3N_4) ceramics and to examine the achievements regarding our understanding of the relationship between processing conditions, chemical composition, microstructure and mechanical properties of Si_3N_4. Si_3N_4 is one of the most important structural ceramics because it possesses a combination of advanced properties such as good wear and corrosive resistance, high flexural strength, good fracture resistance, good creep resistance and relatively high hardness. These properties are obtained through the processing method involving liquid phase sintering in which a tailored microstructure, with high aspect ratio grains and chemistry of intergranular phase, triggers the toughening and strengthening mechanisms leading to the development of high fracture toughness and fracture strength. However, despite high fracture toughness and strength, Si_3N_4 ceramic materials still break catastrophically, and the fracture behaviour of this ceramic is considered to be the major obstacle for its wider use as a structural material. In addition to the macrostructure–mechanical properties relationship, this paper also reviews new designs involving laminates possessing no plane of weakness and some theoretical developments involving crack opening displacement. Proposals of how to improve the fracture resistance were also discussed.

Z. Krstic (✉) · V. D. Krstic
Advanced Ceramics-Mechanical and Materials Department, Queen's University, Kingston, ON, Canada
e-mail: krsticz@queensu.ca

Introduction

In 1994 Poper [1] published a paper on the application of Si_3N_4 ceramics, which was based on computer-searching in the American chemical abstracts system from the years 1967–1992, carried out by the Gmelin Institute (Staffordshire, UK). All suggested applications result from the basic properties of Si_3N_4. These properties were very good refractoriness due to its high thermal shock resistance (low thermal expansion coefficient), chemical inertness to many molten metals, high temperature stability, high wear resistance and abrasiveness due to its hardness, and for ceramic material, relatively high fracture toughness and strength. Summary of the Si_3N_4 material properties are given in Table 1. One of the earliest uses of Si_3N_4 was in the Si_3N_4-bonded refractory brick for blast furnaces in the 1950s. It probably, in terms of the volume used, represents the largest application of Si_3N_4 in industry. In the general field of metallurgy, processes such as continuous casting which requires casting nozzles materials of high durability. Si_3N_4 appears to be very suitable for this application. Berroth et al. [2] reported on application of Si_3N_4-base ceramics in light metal and non-ferrous foundry industry. The applications include components like thermocouple sheaths, heather sheaths, riser tubes, valve seats and plungers, degassing agitators and a number of other specific parts which are in use or recommended and tested to be in use.

Metal cutting is another field of application for Si_3N_4 in which high wear resistance is required. The high thermal shock resistance of Si_3N_4-based cutting tools permits fast machining of cast-iron, steel and Ni-alloys. Tool tips of silicon nitride have been coated with diamond by microwave plasma CVD (chemical vapour deposition) for cutting Al–Si alloys [1].

Table 1 Materials properties of hot-pressed, pressureless sintered and reaction sintered Si_3N_4

Item	Material		
	Hot pressed Si_3N_4	Pressureless sintered Si_3N_4	Reaction sintered Si_3N_4
Density (kg/m^3)	3.07–3.37	2.8–3.4	2.0–2.8
Thermal conductivity (W/m K)	29.3	15.5	2.6–20
Specific heat (J/kg K)	711.756	711.756	–
Flexural strength (MPa)	(20 °C) 450–1200	(20 °C) 275–1000	(1400 °C) ~ 300
	(1400 °C) ~ 600	(1400 °C) ~ 800	(1400 °C) ~ 400
Compressive strength (MPa)	4500	4000	–
Linear thermal expansion ($\times 10^{-6}$/°C)	(20–1000 °C)	(20–1000 °C)	(20–1000 °C)
	3–3.9	~3.5	2.5–3.1
Young's modulus (GPa)	(20 °C) 250–320	(20 °C) 195–315	(20 °C) 100–220
	(1400 °C) 175–250		(1400 °C)120–200
Fracture toughness (MPa m$^{1/2}$)	2.8–12	3.0–10	~3.6

The combination of properties such as temperature and corrosion resistance, thermal conductivity together with a low-specific weight and specific electrical properties make Si_3N_4 suitable for use in a construction of motors as a material for thermal conductors, valves, turbo-charger rotors, gas turbines, catalyst carriers and spark plugs [3]. Since Si_3N_4 is an electrical insulator, its uses for electrical purposes are largely to protect an electrical conductor in the form of an embedded wire or conducting film. Lately, Si_3N_4 has been suggested as a protective coating for high-T_c superconductors. Si_3N_4 has also been considered as a material for nuclear fusion reactors in high temperature gas-cooled reactors and for very high temperature reactors. The main application of Si_3N_4 in semiconductor technology is as the container for molten Si and semiconducting compounds. Thin coatings of Si_3N_4 on quartz vessels reduce the oxygen diffusion into Si. It has also been used in the protection of Si sheets and ribbons for solar cells [1].

In optical fibre technology, Si_3N_4 has been used to protect fibres from moisture and other damaging contaminants by coating them with films of Si_3N_4 by CVD.

Mazzocchi and Bellosi [4], Mazzocchi et al. [5] and Neumann et al. [6] have investigated and reported on the possibility of Si_3N_4 to be used as a biomaterial for orthopaedic implants. At present, Si_3N_4 indeed has become a biomaterial which found its application in spinal implants.

Despite an excellent combination of properties (Table 1), which make Si_3N_4 one of the most important ceramic materials for structural applications, its wider use is limited by Si_3N_4 fracture behaviour which occurs catastrophically. In the last two decades, scientists and researchers have been trying to increase the resistance of crack propagation in Si_3N_4 and to improve its fracture behaviour. The approach was to design a processing condition, in terms of chemical composition and sintering technique capable of providing the conditions for toughening and strengthening mechanisms to take place. In addition to microstructural development, a new structural design, providing conditions for crack deflection and crack bridging, has been an objective of many researchers.

In 1976 a thorough review was conducted by Jack [7] on sialons and related nitrogen ceramics where the emphasis was placed on the effect of processing conditions and chemical composition on fracture strength of these materials. In addition, he suggested an alternative approach using the principles of ceramics "alloying" in the production of "sialons" (phases that had been discovered independently in Japan and England). Jack regarded Si_3N_4 as the first of very wide field of nitrogen ceramics in which there seems to be excellent possibilities on designing materials starting from an atomic scale. At the time, these new oxynitrides included structure types based upon α and β-Si_3N_4, silicon-oxynitride, aluminium nitride, silicon carbide, eucryptite, spinel, melilite and apatite. They were being explored for their thermal, mechanical, chemical and electrical properties.

In 1981 Weiss [8] published a review on silicon nitride ceramics in which he discussed thermodynamics and phase equilibria of these materials. The review includes nitridation of metallic silicon, crystal structure, processing, microstructure and mechanical properties of Si_3N_4, as well as oxidation of Si_3N_4 materials. Weiss also described the relationship between the sintering conditions and the properties of Si_3N_4. The effect of the level of sintering aids on density and chemical composition of secondary phase was also examined in that review. In addition, the relation between grain size, flow size and fracture strength has been reviewed.

In 2007 Hampshire [9] published a review of structure, processing and properties of silicon nitride ceramics. Besides crystalline structure and phase transformations, Hampshire discussed microstructure–property relationships. He stressed

that the amount of additives initially introduced determines the quantity and chemistry of the grain boundary glassy phase which in turn affects such properties as fracture toughness, ambient and high temperature strength, creep resistance and oxidation resistance. As well, Hampshire indicated that, in addition to controlling the nature of the intergranular phase, the morphology of the β-Si_3N_4 is important in determining the strength and fracture toughness of Si_3N_4 ceramics. In the Hampshire's review it has also been shown that, for the same level of porosity, larger volume/number of elongated grains with higher aspect ratio have higher resistance to crack propagation. On the other hand, the number of elongated grains and their aspect ratio are controlled by the level and ration of (Y_2O_3) yttria to (Al_2O_3) alumina sintering aids. In his review, Hampshire examined the significance of volume fraction of the elongated grains on fracture toughness and its effect on toughening mechanisms such as crack bridging, grain rotation and grain pull out. Also, he pointed out that high fracture resistance and high fracture strength can be developed in self-reinforced Si_3N_4 by controlling the size and volume fraction of β-Si_3N_4 grains with high aspect ratio well-dispersed in fine-grained matrix.

Crystal structures of Si_3N_4

Silicon nitride exists in two major crystalline forms: α- and β-phase. α-Si_3N_4 is the low temperature modification and β-Si_3N_4 is the high temperature modification. Both phases have a hexagonal crystal structure. The lattice parameters of α-Si_3N_4 are $a = 7.7541(4)$ Å, and $c = 5.6217(4)$ Å, with an atomic layer sequence of ABCD (Fig. 1); the corresponding parameters for β-Si_3N_4 are $a = 7.6044(2)$ Å, $c = 2.9075(1)$ Å, and an atomic layer sequence of ABAB (Fig. 1) [10–12]. Both structures are built up from a SiN_4 tetrahedron and can be transformed into each other by a 180° rotation around an axis normal to the C direction (Fig. 2). At normal pressures, Si_3N_4 does not melt but dissociates at around 1877 °C according to the reaction [3]:

$$Si_3N_4\,(\text{solid}) \rightarrow 3Si\,(\text{liquid}) + 2N_2\,(\text{gas}) \qquad (1)$$

Sintering of Si_3N_4 ceramics

Si_3N_4 ceramics are usually sintered to high density using pressure sintering techniques such as hot-pressing (HP) and hot-isostatic-pressing (HIP), and pressureless sintering technique where densification of the powders occurs without the application of external pressure. The pressureless sintering method is preferred since complex-shaped components can easily be densified and the cost of the products is significantly lower.

In order for sintering to take place, two conditions must be met: (1) the diffusion rate of the atoms must be high, and (2) the energy of newly formed grain boundaries must be sufficiently low to cause a decrease in system free energy [13].

The activation energy required for self-diffusion of covalent bonded solids, such as Si_3N_4, is extremely high and self-diffusion coefficients are, therefore, low. Since appreciable shrinkage of the powder compacts can occur only when matter is transported to the surfaces of pores by volume and grain boundary diffusion, it is predicted that there will be little material transport in these covalently bonded solids [14]. This, combined with very high grain boundary energy of pure Si_3N_4, makes its densification very difficult even at a very high temperature and for a long time. Therefore, sintering aids are always needed to bring down the grain boundary energy of Si_3N_4 and to increase diffusivity. Every powder particle of Si_3N_4 contains a surface layer of SiO_2 which during sintering reacts with sintering aids, oxide additives, and some of the nitride itself. At sintering temperatures, this reaction forms a liquid phase which promotes densification first by rearrangement and at the same time by solution of α-Si_3N_4 into the liquid phase and then by precipitation of β-Si_3N_4. The term liquid-phase sintering is used to describe the sintering process when a portion of material being sintered is in the liquid phase. In liquid-phase sintering, the liquid provides the vehicle for rapid mass transport and thus rapid densification. The driving force for densification is the capillary pressure of the liquid phase between the fine solid particles [15]. Furthermore, the kinetics of densification in solution-precipitation stage of sintering is much higher then in the solid state sintering. In liquid phase sintering the diffusion occurs in the liquid where the diffusivities are order of magnitude higher then those in the solid state sintering [15]. In this stage of sintering shrinkage follows the equation [16, 17]:

$$\frac{\Delta L}{L_0} = \frac{1}{3}\frac{\Delta V}{V_0} = \left[\frac{12 \cdot \delta \cdot D \cdot C \cdot \gamma_{LV} \cdot \Omega}{k \cdot T}\right]^{1/3} r^{-4/3} \cdot t^{1/3} \qquad (2)$$

where r is the radius of the particle, D is diffusion coefficient of the solid in the liquid, T is the absolute temperature, k is the gas constant, δ is the width/thickness of the liquid film between the grains, C is the solubility of the solid in the liquid, Ω is the atomic volume, t is the sintering time and γ_{LV} is the liquid–vapour interfacial energy.

With the purpose of determining the diffusion coefficient of Si_3N_4 during the liquid phase sintering, in 2002, Krstic and Krstic [18] experimented with isothermal sintering of Si_3N_4 containing $\sim$10 wt% oxide additives ($Y_2O_3 + Al_2O_3$). The sintering was carried out at 1780 °C for 20, 45, 60, 90 and 120 min. The result of isothermal

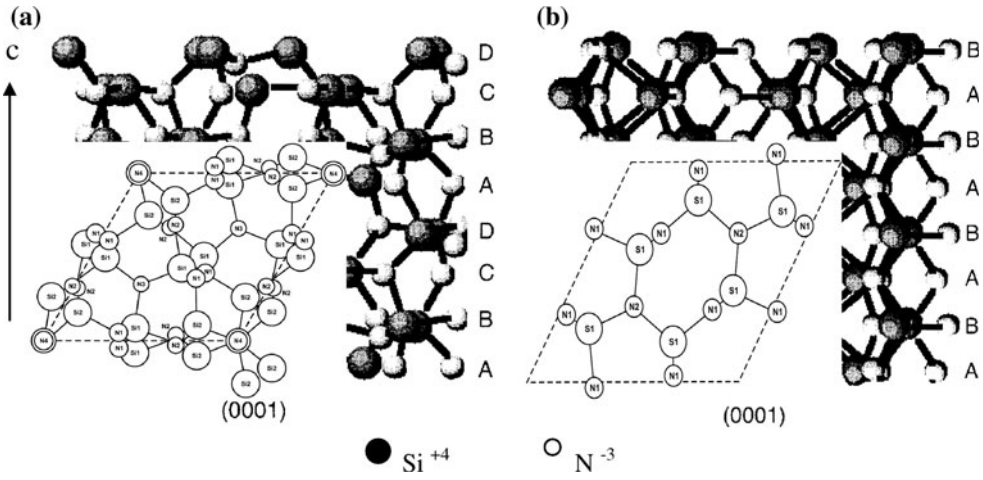

Fig. 1 Crystal structures of **a** α-Si_3N_4 and **b** β-Si_3N_4

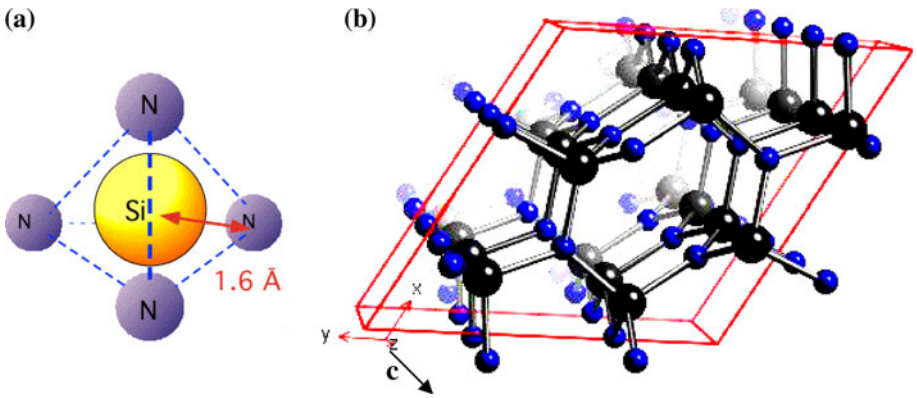

Fig. 2 Crystal structure of **a** SiN_4 tetrahedron and **b** unit cell of SiN_4. Bigger ions are silicon; smaller ions are nitrogen

sintering was plotted in terms of log-shrinkage and -sintering time (Fig. 3) in order to determine the slope of the curve.

From the graph in Fig. 3 it was determined that the slope of the straight line is $\sim 1/3$ confirming the validity of Eq. 2. Based on the experimentally determined slope of the curve and knowing other values in Eq. 2, it was possible to estimate the diffusion coefficient responsible for mass transport. Introducing values for $\delta = 4 \times 10^{-10}$ m, $\Omega = 4.36 \times 10^{-28}$ m^3, $C = 0.8$–0.95, $\gamma = 8.5$ J/m^2, and $r = 2.4 \times 10^{-7}$ m, the diffusion coefficient of Si_3N_4 at 1780 °C was estimated to be in the range from 10^{-13} to 6.39×10^{-12} cm^2/s.

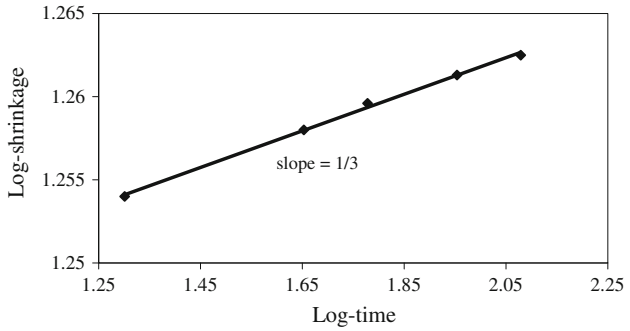

Fig. 3 Log-shrinkage versus log-sintering time

In 1980, Thummler [19] reported values for the self-diffusion coefficient at 1300–1400 °C between 3×10^{-18} and 5×10^{-19} cm^2/s, which is 5–6 orders of magnitude lower than the measured values reported in Fig. 3 (i.e., at 1780 °C). Considering that the diffusion coefficient is 3–5 orders of magnitude lower than that of a substance in a liquid, the value of 10^{-13} to 6.39×10^{-12} cm^2/s determined in these experiments is considered reasonable.

Not only the presence of liquid phase during sintering has a significant affect on Si_3N_4 diffusion rate and in turn on its sinterability, but also on the phase transformation in Si_3N_4.

$\alpha \rightarrow \beta$ phase transformation in Si_3N_4

The presence of a liquid phase during sintering of Si_3N_4 is also important for the $\alpha \rightarrow \beta$ phase transformation which is believed to occur after dissolution of the fine α particles in the liquid phase formed between sintering aids and subsequent

precipitation of the β nuclei [20]. For the formation of β phase from α phase, layer C must be changed to layer A and layer D must be changed to layer B (Fig. 1) [21]. This reconstruction of the crystal structure requires short-range diffusion rather than simple translation, and diffusion occurs as a result of the concentration gradient of α-Si_3N_4 rich powders. The diffusion of silicon and nitrogen takes place through the liquid phase followed by precipitation of β phase in the form of small nuclei on the existing β-Si_3N_4 grains (Fig. 4).

Another outcome of this analysis indicated in Fig. 4 is that, regardless of the initial phase composition of the powder, if there is a sufficient amount of liquid phase during sintering, the α–β phase transformation will be complete, resulting in final structure consisting of only elongated β-Si_3N_4 phase. As a consequence, it is expected that with prolonged heating time at sintering temperatures, β-Si_3N_4 grains which are in equilibrium with the reactive liquid, will grow anisotropically. The growth of elongated β-grains in the presence of a liquid can be controlled either by the diffusion of the atoms through the liquid or by reaction at the grain/liquid interface. For those two mechanisms of grain growth, (diffusion control and interface-reaction control), a kinetic equation was developed [23, 24] and is known as the LSW theory:

$$D^n - D_0^n = K_D \cdot t \tag{3}$$

where D is the average grain size, D_0 is the initial grain size, n is the growth exponent, K is the rate constant and t is the time. The rate constant K and growth exponent n are different for the length and width directions of the β-Si_3N_4 grains. The aspect ratio, length/width, was defined as [25]:

$$\mathrm{AR} = \frac{L}{W} = \left(\frac{K_L^{1/3}}{K_W^{1/5}}\right) \cdot t^{(1/3-1/5)} = \left(\frac{K_L^{1/3}}{K_W^{1/5}}\right) \cdot t^{2/15} = \left(\frac{K_{OL}^{1/3}}{K_{OW}^{1/5}}\right) \cdot t^{2/15} \exp\left[\frac{\left(\frac{Q_L}{3} - \frac{Q_W}{5}\right)}{kT}\right] \tag{4}$$

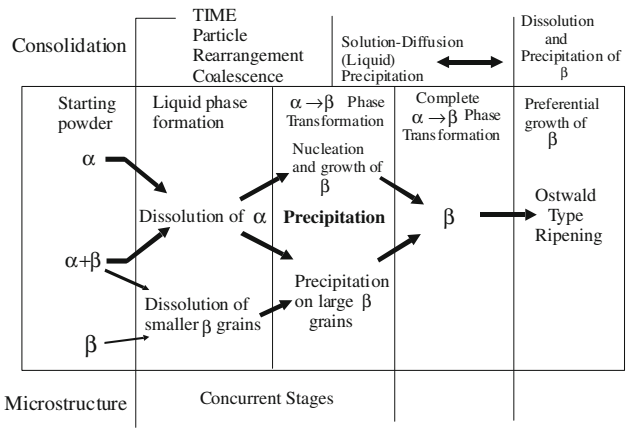

Fig. 4 $\alpha \rightarrow \beta$ microstructure change and phase transformation during liquid phase sintering of Si_3N_4 [22]

where L is the average length of the β-Si_3N_4 grains, W is the average width of the β-Si_3N_4 grains, K_L and K_W are the rate constants in the length and width direction of the β-Si_3N_4 grains, Q_L and Q_W are the activation energies ($Q_L = 686$ J/mol and $Q_W = 772$ J/mol for length and width, respectively), k is the gas constant, t is the time and T is the absolute temperature. Lai and Tien [26] showed that the growth exponent n equals 3 in the length direction and 5 in the width direction. Due to the prismatic configuration of β-Si_3N_4 grains, the growth of length in the C direction [0001] is controlled mainly by the solute diffusion through multigrain junctions, while the growth of width in the [2100] direction is controlled by the diffusion along grain boundaries. According to this, the growth rate in the width direction is lower than the growth rate in the length direction, resulting in the formation of elongated β-Si_3N_4 grains. Figure 5 shows a bi-modal microstructure of Si_3N_4 sintered pressureless sintered and hot isostatically pressed (HIP) with Y_2O_3 and Al_2O_3 consisting of elongated β-Si_3N_4 grains and a matrix with slightly elongated and equiaxed grains. As expected the thickness and the aspect ratio were found to develop in a pressureless sintered samples and significantly smaller grains in HIP-ed samples. It is not surprising that HIP-ed material exhibits higher strength and hardness with minimal or no increase in fracture toughness. Elongated grains with large aspect ratio are the key to high fracture toughness of β-Si_3N_4.

Over the last decade large effort was centered on atomic-level structural modelling in order to understand the mechanism of growth of elongated grains which are the key to toughening and strengthening of silicon nitride ceramics. A series of papers conducted by Painter and co-workers [28, 29] have shown that the formation of elongated grains is sensitive to cations used as the sintering additives. For example, using aberration corrected Z-contrast scanning transmission electron microscopy Shibata et al. [30] have shown that La (lanthanum) atoms preferentially segregate to the crystalline interfaces rather than within the amorphous film located at the grain boundaries. The significance of the atomic level study of the dopants distribution at the grain boundaries has been confirmed from the study of the adsorption of La atoms at the prism plane of β-Si_3N_4 employing self-consistent partial-wave method [31]. Similarly, using the example of Lu (lutetium) doped Si_3N_4 ceramics, it has been shown that the transition from crystalline to amorphous region at the interface is not atomically abrupt but is composed of sub-nanometer-scale ordered regions [32].

Si_3N_4 sintering aids

The mechanical properties of Si_3N_4 ceramics strongly depend on the sintering conditions. The type of aids used to

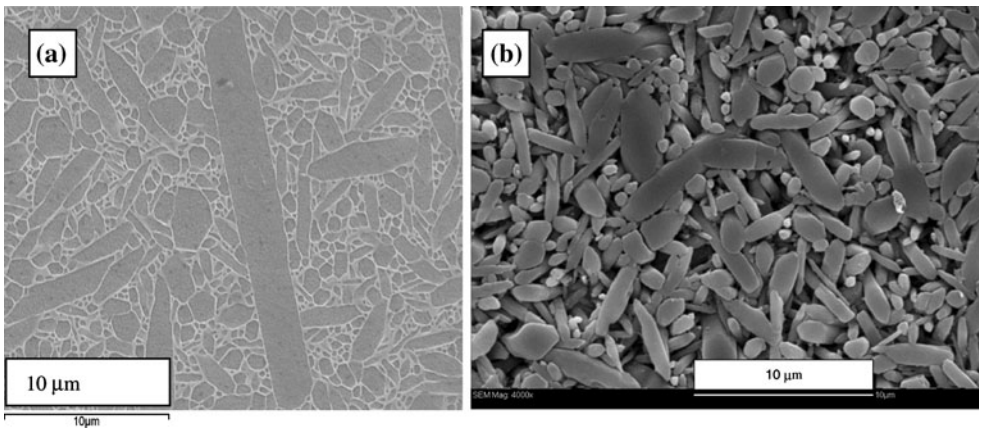

Fig. 5 Bi-modal microstructure of Si_3N_4 sintered with Y_2O_3 and Al_2O_3 additions **a** pressureless sintered at 1780 °C, plasma etched Si_3N_4, **b** HIP-ed Si_3N_4 at 1760 °C, and chemically etched [27]

sinter Si_3N_4 determines density and the chemical composition of the grain boundary phase. Other factors, such as the amount of the liquid phase and the heat treatment, influence the grain size and grain morphology as well. The chemistry of the liquid phase, along with the characteristics of the initial powder and processing conditions, are the key factors which determine the microstructure and properties of Si_3N_4 ceramics.

Magnesium oxide (MgO) was the first sintering additive ever used to densify Si_3N_4 ceramics [33]. Beside MgO, other sintering aids were also used including (Y_2O_3) [34, 35], alumina (Al_2O_3) [36, 37], beryllia (BeO) [38], zirconia (ZrO_2) [39], ceria (CeO_2) [40], hafnia (HfO_2) [41], ytterbium oxide (Yb_2O_3) and silica (SiO_2) [42], alumina and calcium oxide (CaO) [43], yttria and neodymium oxide (Nd_2O_3) [44], Y_2O_3 and SiO [2, 45] lanthanum oxide (La_2O_3) and niobium carbide (NbC) [46], etc. Amongst all oxide sintering aids the best-known system is the yttria–alumina (Y_2O_3–Al_2O_3).

Besides oxides, a number of metals, such as calcium (Ca), iron (Fe), manganese (Mg) and their mixtures were used as sintering aids [47].

Si_3N_4 microstructure–chemical composition–fracture toughness relationship

Microstructure evolution during sintering and its effect on mechanical properties of the Si_3N_4 ceramics, especially fracture toughness, has been the subject of many investigations in the last two decades. Some researchers believe that the width of the grains plays the most important role in determining the mechanical properties of Si_3N_4 ceramics [48]. Others believe that the aspect ratio of the elongated grains is the prevailing microstructural feature which determines mechanical properties of these ceramics [49]. In 1991, Lai and Tien [26] showed that the fracture strength and fracture toughness of Si_3N_4 ceramics with 10 wt% oxide additives (Y_2O_3 + Al_2O_3), sintered under 10 atm pressure of nitrogen, depend on the aspect ratio of the β-Si_3N_4 grains (Fig. 6). Even though the tendency of the Si_3N_4 to grow elongated grains has been observed for a long time [50], the control of the process towards the maximization of the fracture toughness is relatively recent. Lange [51] in 1979 reported an improvement of fracture strength and fracture toughness to the level of $K_{IC} = 6$ MPa $m^{1/2}$ when the β-Si_3N_4 grains with high aspect ratio were formed during sintering. In 1986 Woetting et al. [52] produced Si_3N_4 with 15% Y_2O_3 and 3.4% Al_2O_3 having a K_{IC} of 7.8 MPa $m^{1/2}$ (measured by micro-indentation technique). Tani et al. [53] obtained elongated Si_3N_4 grains in the Si_3N_4–Y_2O_3–Al_2O_3 system having a toughness of 6 MPa $m^{1/2}$ (measured by chevron notch technique). Compositions containing less liquid phase (5% Y_2O_3 and 1.13% Al_2O_3) and densified by a hot isostatic pressing (HIP) technique achieved a fracture toughness of 8.2 MPa $m^{1/2}$ [54]. Similar compositions (5% Y_2O_3 and 2% Al_2O_3) were also investigated by Mitomo et al. [55]. Their materials were heated under a nitrogen gas pressure of 980 kPa at 1950 °C for 1 h, producing a grain aspect ratio of 4.2. The fracture toughness of these materials, fabricated from α and β powders, ranged from 5.8 to 6.3 MPa $m^{1/2}$. Using a single-edge-pre-cracked beam method Neil et al. [56] reported a value for K_{IC} of 5.5 MPa $m^{1/2}$ for a hot pressed composition containing 6% Y_2O_3 and 1.5% Al_2O_3.

The effect of the aspect ratio of β-Si_3N_4 grains on mechanical properties of Si_3N_4, ceramics, sintered with different amounts of oxide additives (Y_2O_3 + Al_2O_3) and different oxide compositions (Y_2O_3/Al_2O_3), has been systematically investigated and reported by Krstic and Krstic [57, 58] who showed that the aspect ratio of elongated grains is the most important factor in controlling mechanical properties in these ceramics.

Strengthening and toughening of Si_3N_4

Owing to the brittle nature of Si_3N_4, over the years, there has been a continuous interest in exploring a variety of

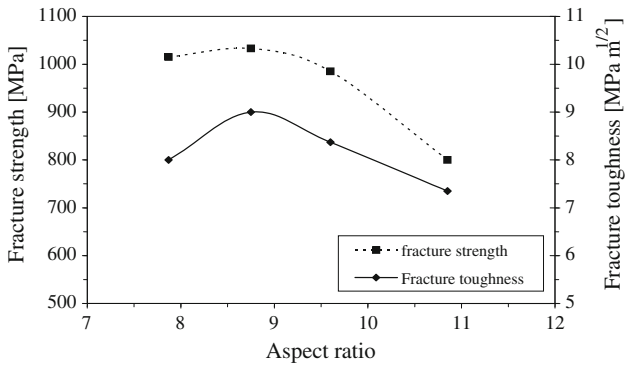

Fig. 6 Microstructural dependence of fracture strength and toughness of Si_3N_4 ceramics [26]

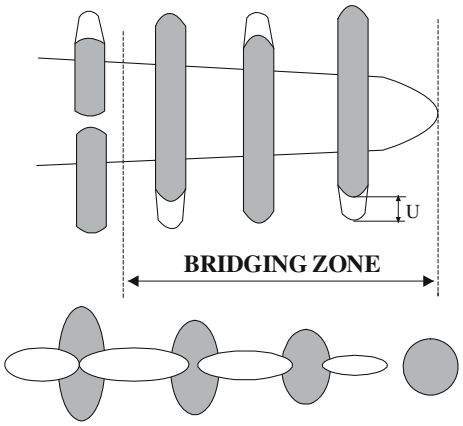

Fig. 7 Crack bridging, in which unbroken ligaments are left behind the crack tip. The *upper figure* shows frictional bridges, while the *lower figure* shows ductile bridges

approaches for enhancing its fracture toughness and reliability. In general, fracture of brittle materials involves very little dissipation of the applied strain energy by processes other than breaking of the atomic bonds. In extremely brittle systems, the fracture surface energy often approaches the bonding energy. By employing an energy rate criterion Griffith [59, 60] showed that the critical stress for crack extension (the fracture strength) is:

$$\sigma_f = \sqrt{\frac{2E\gamma_{eff}}{\pi c}} \tag{5}$$

where c is the half length of the elliptical crack, γ_{eff} is the fracture surface energy or fracture toughness and E is the Young's modulus. Equation 5 shows that the strength of a real material depends on the size of the crack present in the structure.

Over the years, a variety of approaches have been used to enhance the fracture toughness of ceramics. The basic idea behind all toughening mechanisms is to develop a microstructure capable of reducing the crack tip stress field and increasing the applied stress required for crack extension.

The two most important mechanisms of toughening in the so-called self-reinforced Si_3N_4 ceramics are crack bridging (Fig. 7) and crack deflection (Fig. 8). Whether or not the above two mechanisms of toughening will be operational depends on the interface between the elongated β-Si_3N_4 grains and the surrounding intergranular phase. To promote crack bridging and deflection, the interface must break down and allow elongated β-Si_3N_4 grains to pull out as the crack front approaches them. The relationship between the fracture toughness and the interfacial strength is given by the equation [49]:

$$K_{IC} = K_m \cdot (1 - V) + \left\{ \frac{4E\tau Vu}{(1 - \nu^2)} \cdot K_m \right\} \cdot \frac{l}{d} \tag{6}$$

where K_{IC} is the total fracture toughness, K_m is the fracture toughness of the matrix (with equiaxed grains), V is the volume fraction of the elongated grains, u is the pullout length, τ is the strength of the interface, E is the Young's modulus, ν is the Poisson's ratio and l/d is the grain aspect ratio.

Recently, using Eq. 6, Krstic [49] has shown that theoretically it is possible to achieve fracture toughness as high as 46.3 MPa $m^{1/2}$, provided that all elongated grains are perpendicular to the crack plane and thus all contribute to the toughening.

Crack deflection is defined as a twist and tilt of the crack front between microstructural elements (Fig. 8), which reduce the stress intensity at the crack tip.

The fracture toughness increment by pull-out can be expressed by Eq. 7 [62]:

$$K_{IC}^{p} = K_m^{p} \sqrt{\frac{1}{(1 - V_p)A} \left[1 + 2\left(\frac{2V_p(l/d)\tau}{\sigma} \right)^3 \right]} \tag{7}$$

where K_{IC}^{p} is the overall fracture toughness due to pull-out, K_m is the fracture toughness of the matrix without pull-out, A is a constant, τ is the strength of the interface and σ is the fracture strength. l and d have the same meaning as in Eq. 6. Close inspection of Eqs. 6 and 7 show that a high-volume fraction of reinforcement phases with high-aspect ratio is required for toughening.

For rod-shaped reinforcing particles, the fracture toughness, due to the local deflection of a planar crack by these reinforcing particles, can be expressed by Eq. 8 [61] of the form:

$$K_{IC}^{d} = K_m \cdot \sqrt{1 + V_p((0.6 + 0.007(l/d) - 0.0001(l/d)^2)} \tag{8}$$

where K_{IC}^{d} is the fracture toughness due to crack deflection, K_m is the fracture toughness of the matrix without crack

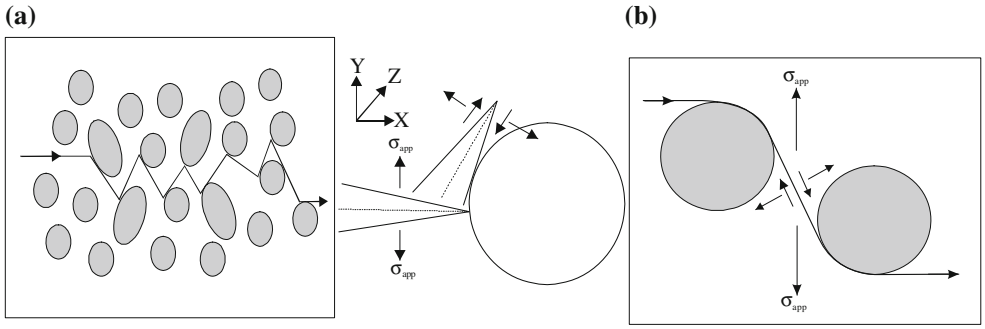

Fig. 8 Schematics of crack deflection **a** the crack path tilts to avoid obstacles and **b** the crack front twists to by-pass obstacles [61]

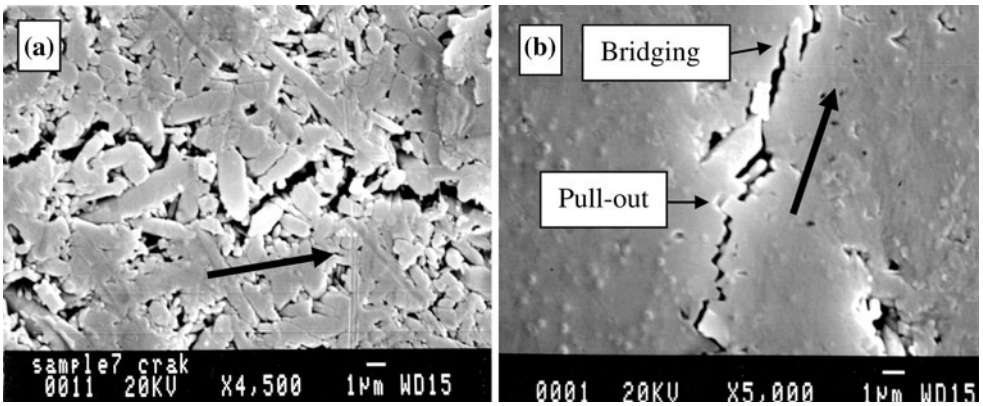

Fig. 9 Crack profiles from indentation cracks in Si_3N_4 sintered at 1780 °C with oxide additives of ~10 wt% **a** crack deflection, **b** crack deflection and pull-out (*black arrows* show direction of crack propagation) [58]

deflection, V_p is the volume fraction of rods, l is the length of the rods, d is the diameter of the rods and l/d is the aspect ratio.

Figure 9 shows crack deflection, crack pull-out and crack bridging operating simultaneously in Si_3N_4 sintered with Y_2O_3 and Al_2O_3 additives. As already mentioned, these mechanisms operate most effectively in systems with β-Si_3N_4 elongated grains of high aspect ratio as is the case for the composition with ~10 wt% additives (7 wt% Y_2O_3 and 3 wt% Al_2O_3). In microstructures with equiaxed grains, the contribution of this mechanism is expected to be minimal.

Although the static fracture toughness measurements method, based on linear-elastic fracture mechanics method, has been well-suited for fracture toughness determination in equiaxed grain structures its application to ceramics with highly developed process zone such as fully or partially stabilized zirconia or silicon nitride with large pull-out and crack bridging zone has been highly controversial. Even the most carefully made *R*-curve measurements could not accurately assess the initial toughness point. This is best illustrated with the example of silicon nitride doped with rare-earth elements such as La, Gd (gadolinium) and Lu [63]. In this context, rigorous and approximate methods were proposed for determining the onset of fracture in materials with steeply raising *R*-curves. These methods are based on the crack opening displacement concept on Vickers indented cracks [64].

Unified approach to fracture of ceramics

Since the development of energy rate theory expressed in the form of a Griffith [59] equation, there has been continuous interest to broaden the concept of energy rate theory to include the effects of microstructural features such as porosity, grain size and residual stresses. Although the Griffith equation has been successfully used to predict the strength of a homogenous pore- and residual stress-free material, when it comes to a non-fully dense polycrystalline and anisotropic materials, the theory does not explain the effect of any of the key microstructural features. Over the last several decades, a number of papers have been published on the effect of porosity [65–69], grain size [70, 71] and residual stresses [72–74] on the strength of ceramics. All of these studies were centered on the role of each microstructural feature in strengthening of ceramics independent from the effect of others. By adopting a stress

intensity factor approach and based on crack opening displacement concept, in 1998 a unified approach to the fracture of brittle materials was proposed which incorporates the effects of porosity, grain size and anisotropic residual stresses in the form of a continuous model [75, 76].

It is now well-accepted that fracture of ceramics and brittle materials originates either from a single pore of the largest size or from the cluster of pores linked together to create a largest size pore [77]. In the past, many empirical and semi-empirical models were used to correlate porosity to strength of a porous ceramic but failed to explain why an increase in porosity leads to an increase in strain. By adopting the concept of crack opening displacement it was possible to account for the increase displacement/strain of the material under the same applied stress in which not only pore volume fraction but also the pore size and inherent flaw size play role in controlling fracture strength of a porous ceramics (Fig. 10). In this concept the total crack size responsible for fracture, C, consists of pore size, D, and flaw size, s.

Based on this concept, it has been shown that the relationship between the number of pores per unit volume N^{p} (related to the pore volume fraction V and pore radius R through the equation $N^{p} = 3V/4\pi R^{3}$) is given by the equation [77]:

$$E = E_0\left\{1 + 16[(1 - \nu^2)N^{p}R^{3}\Phi]/3\right\}^{-1} \quad (9)$$

where $\Phi = (1 + s/R)^3 + 9/2(7 - 5\nu)(1 + s/R)^2 + (4 - 5\nu)/2(1 - 5\nu)$, ν is the Poisson's ratio and E_0 is the Young's modulus of a pore-free ceramics.

In terms of pore volume fraction the Young's modulus is expressed as:

$$E = E_0\left[1 + 4V\left(1 - \nu^2\right)(1 + s/R)^3/\pi\right]^{-1} \quad (10)$$

Note that in Eq. 9 Φ is assumed to be equal to 1. The change of Young's modulus as a function of pore volume fraction and pore radius is illustrated in Fig. 11.

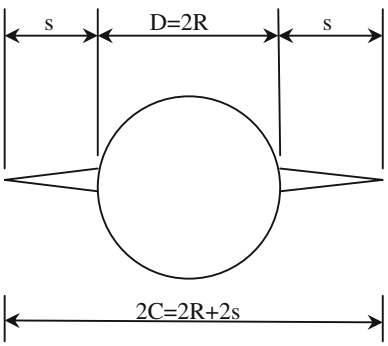

Fig. 10 Relation between pore size, D, and an annular flaw size, s

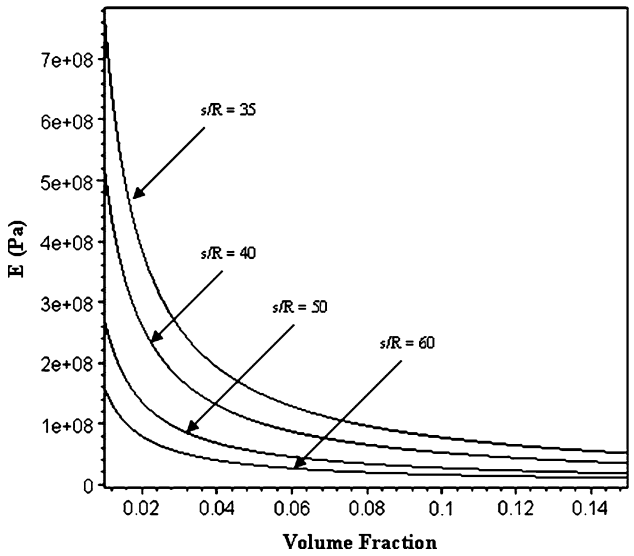

Fig. 11 Predicted variation of Young's modulus with pore volume fraction, pore radius and inherent flaw size

The key result of this theoretical approach is the finding that, for a given pore volume fraction, the level of Young's modulus decrease with porosity depends critically on the pore radius and the annular/inherent flaw size present in the material. With this theoretical model it was possible to predict the variation of Young's modulus with pore volume fraction in many materials including metallic materials like nanocrystalline palladium. More specifically, it was possible to explain why nanocrystalline palladium with a lower pore volume fraction can have lower Young's modulus (if it contains larger cracks/inherent flaw size) and nanocrystalline palladium with higher pore volume fraction can have higher Young's modulus (see Fig. 12) (if it contains smaller size inherent flaws) [67]. Here, it should be noted that nanocrystalline palladium possesses limited plasticity and fractures in a brittle fashion just like most polycrystalline ceramics.

The validity of the crack opening displacement concept was confirmed by using Embedded-Atom Model on a single-crystal Ni cluster of 4000 atoms arranged in a cubic form [78].

Somewhat different behaviour was observed in porous silicon nitride ceramics with porosity level varying for 0.4% to over 6 vol% [79] as presented in Fig. 13. Figure 13 shows that as the pore volume fraction increases so does the pore size and the flow size and thus proper characterization of a porous silicon nitride must include the variation of pore size and the inherent flaw size. For example, at low level of porosity (0.5%) the flaw size is much smaller that the pore size ($s/R = \sim 0.1$) and at higher level of porosity (6%) the flaw size is larger than the pore size ($s/R = \sim 2.5$).

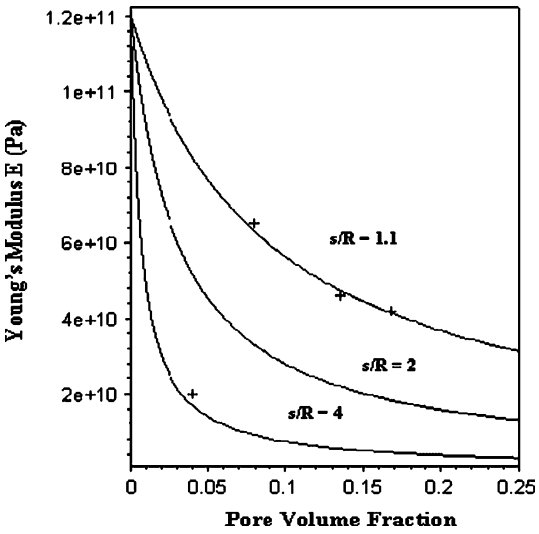

Fig. 12 Predicted and measured Young's modulus of nanocrystalline palladium as a function of pore volume fraction, pore size and inherent flaw size (measured values for the Young's modulus are taken from Ref. [77])

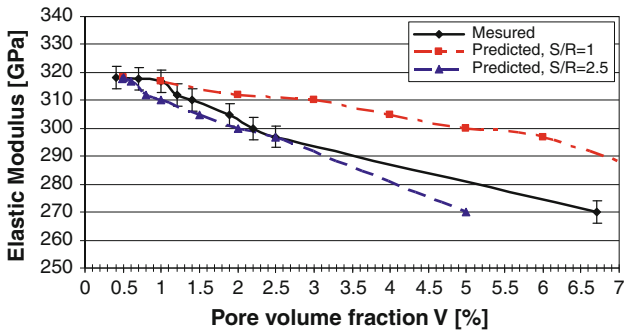

Fig. 13 Effect of porosity on elastic modulus of Si_3N_4 sintered with Y_2O_3 and Al_2O_3 additions. Predicted values for Young's modulus were obtained based on $E_0 = 320$GPa, $\nu = 0.18$, $\gamma_{eff} = 40$ J/m^2, $s/R = 1$, and $s/R = 2.5$ [27, 77]

Following the same pore-size inherent flaw-size concept, and assuming that the reduction in strain energy stored in the porous ceramics is due to a decrease in Young's modulus in the presence of pores, the theory was extended to explain the fracture strength-porosity relationship [76]:

$$\sigma_f = \left[\pi\gamma E_0/D\left(1-\nu^2\right)\right]^{1/2}\left[1+16(1+s/R)N^p\left(1-\nu^2\right)R^3/3\right]^{-1/2} \quad (11)$$

Replacing the number of pores per unit volume with pore volume fraction (V) and pore diameter (R) Eq. 11 takes the form:

$$\sigma_f = [\pi\gamma E_0/D(1+s/R)]^{1/2}[1+4V(1+s/R)/\pi]^{-1/2} \quad (12)$$

The predicted variation of strength (based on Eq. 12) with pore volume fraction, pore size and the inherent flaw size is shown in Fig. 14, along with experimentally measured strength for porous silicon nitride [79]. Identical to Young's modulus-dependence on porosity, there are three equally important factors which control the strength of a porous ceramics, i.e. pore volume fraction, pore size and the inherent flaw size.

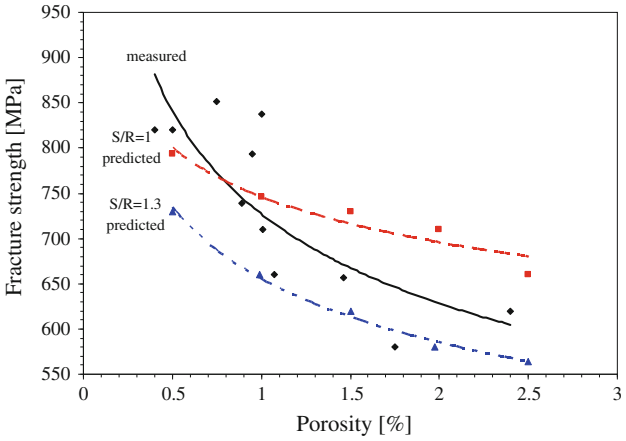

Fig. 14 Effect of porosity on fracture strength of Si_3N_4 sintered with Y_2O_3 and Al_2O_3. Predicted values for fracture strength were obtained based on $E_0 = 320$ GPa, $\nu = 0.18$, $R = 30$ μm, $\gamma_{eff} = 40$ J/m^2, $s/R = 1$ and $s/R = 1.3$ [76, 80]

Inspection of Fig. 14 shows that along with an increase in pore volume fraction there is an attendant increase in inherent flaw size. For example, at low porosity volume fractions (<1%), the flaw size is approximately equal to the pore size ($s/R = 1$) and as the porosity volume fraction increases to >2 vol% the flaw size increased to by 30% compared to the pore radius ($s/R = 1.3$).

Application of the theory to fracture of polycrystalline ceramics

The crack opening displacement concept was further extended to incorporate fracture of polycrystalline ceramics possessing thermo-elastic anisotropy and fracture of brittle matrixes with second phase particles having different thermal and elastic properties from that of the matrix [70, 71]. For the purpose of this analysis, ceramic materials are classified into two structural categories; isotropic and anisotropic, depending on whether or not they have a cubic or non-cubic structure. This division is based on the theoretical analysis and experimental findings [70, 71] which show that there is quite different fracture response between anisotropic and isotropic polycrystalline ceramics. For example, it was observed that the anisotropic ceramics show strong grain size dependence whereas isotropic ceramics show weak or no dependence of fracture stress with grain size, at least for grain sizes ranging from a few microns to several hundred microns [72].

The concept of crack opening displacement can best be understood by considering a cavity situated in a polycrystalline ceramic of the same size and shape as the grain, as illustrated in Fig. 15. For the case of a randomly oriented grain structure it is expected that, statistically, there will be at least one cluster of grains in which the central grain with axis of minimum thermal expansion is perpendicular to the axis of maximum thermal expansion of the surrounding grains. On cooling from high temperature this grain orientation will place the central grain under compressive stress and the surrounding grains under tensile stress. This will favour opening of the annular crack around the grain and be responsible for fracture of the ceramic. The compressive stress developed within the central grain is given by the expression [81]

$$P = 2E(\alpha_{\max} - \alpha_{\min})(T_{\max} - T_{\min})/3(1 - v) \quad (13)$$

where $\alpha_{\max}$ is the linear thermal expansion in the direction of highest expansion/contraction, $\alpha_{\min}$ is the linear thermal expansion in the direction of lowest thermal expansion/contraction, $T_{\max}$ is the temperature from which the ceramic is cooled and $T_{\min}$ is the temperature to which the ceramic is cooled. Based on this grain configuration, the expression for the strength of an anisotropic ceramic is developed [72, 76]:

$$\sigma_f = \left[\pi E_0 \gamma_{\text{eff}}/G(1 - s/r)(1 - v)^2\right]^{1/2} - AP\Phi_t \quad (14)$$

where G is the grain diameter, r is the grain radius, s is the inherent flaw size, A is a constant that takes into consideration of the level of residual stress relaxation and

$$\Phi = \left\{1 - \left[1/(1 + s/r)^2\right]^{1/2} + \left[1/2(1 + s/r)^{5/2}\right]\left[1 - 1/(1 + s/r)^2\right]^{1/2}\right\} \quad (15)$$

The significance of Eq. 15 is that it embodies the effects of grain size, inherent/annular flaw size and anisotropic residual tress on strength of a polycrystalline anisotropic ceramic into a single equation. The key result of the above theory is that the inherent flaw size and the grain size are not necessary equal in size and that the reduction in grain size does not necessary lead to the reduction in flaw size responsible for fracture. This is illustrated in Fig. 16 which shows the change of fracture strength as a function of grain size in polycrystalline alumina [82].

Inspection of Fig. 16 shows that the strength of alumina can vary widely for the same grain size depending on the inherent or (often called) processing flaw size. For example, samples with grain sizes of <1 μm have lower strength than the samples with grain sizes of 4 μm simply because samples with grain size of <1 μm contained larger flaw sizes. This has an important practical implication in that the high strength alumina can be fabricated not only by keeping the grain size low but by keeping both the grain size and the flaw size small. Again, this finding confirms the assertion introduced earlier that the grain size and the flaw size are the two independent microstructural features.

Application of the theory to thermal shock fracture-porous material

Homogeneous and isotropic material

Since Hasselman [83] thermal shock theory, which describes the role of thermal expansion coefficient and flaw size in the fracture of brittle materials, there has been continued interest in expanding the theory to include the effect of porosity and anisotropic stresses on fracture. One obvious approach to incorporating the effect of porosity into the equation for thermal shock is by adopting the same concept of crack-pore configuration as in Fig. 10 which assumes that the crack size responsible for fracture consists of pore radius and inherent flaw size $C = R + s$. In this approach, fracture of a porous, isotropic single phase material occurs when a crack ($C = R + s$) reaches a critical size or the residual quenching stress $P = \alpha E\Delta T/(1 - 2v)$ reaches a critical value [75]. Based on this, an

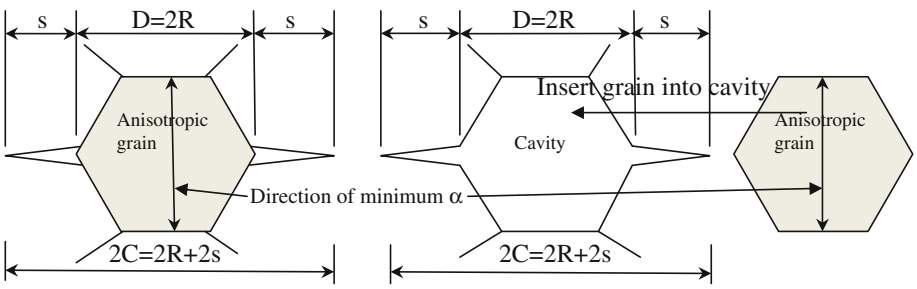

Fig. 15 Schematic of a hexagonal grain being inserted into the cavity of the same size and shape at high temperature. Assuming that the surrounding grains are oriented such that their direction of maximum thermal expansion is perpendicular to the central grain, on cooling from high temperature, the central grain will be under compression and surrounding grains will be under tension

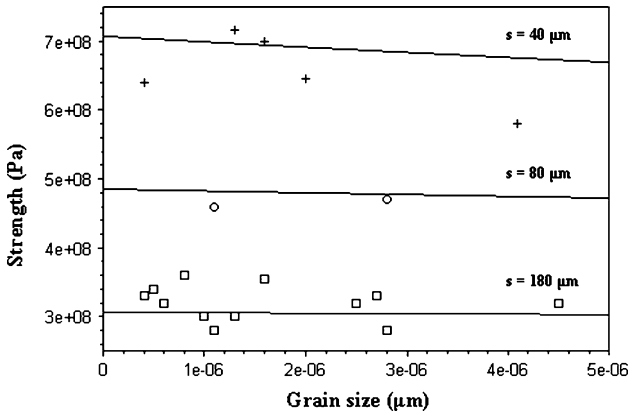

Fig. 16 Predicted (from Eq. 6) and measured flexural strength of polycrystalline alumina. Measured values for strength are taken from Ref. [82]

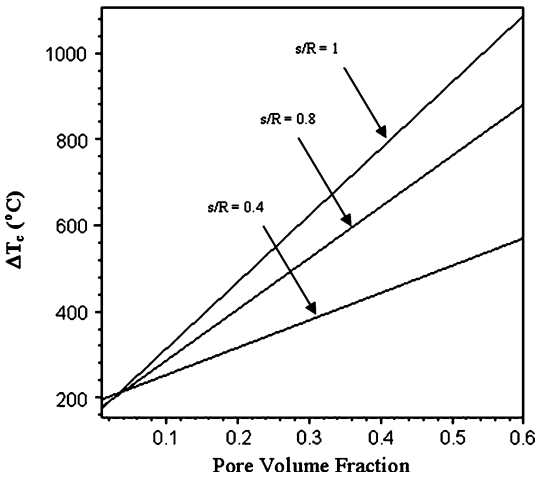

Fig. 17 Predicted change of critical temperature drop with pore volume fraction and *s*/*R* for a homogeneous single phase ceramic

equation for a critical temperature difference ΔT_c was developed:

$$\Delta T_c = \left[\pi\gamma_{\text{eff}}(1-2\nu)^2/2(R+s)\alpha^2 E_0\left(1-\nu^2\right)\right]^{1/2} \left[1+16\left(1-\nu^2\right)N^{\text{p}}(R+s)^3/3\right] \quad (16)$$

where α is the linear thermal expansion, γ_{eff} is the effective fracture surface energy, N^{p} is the number of pore per unit volume (equivalent to pore volume fraction, $N^{\text{p}} = 3V/4\pi R^3$), R is the pore radius and E_0 is the Young's modulus of a pore-free material. Equation 16 and Fig. 17 show that the thermal shock resistance of a material is controlled not only by the flaw size (inherent flaw size in Eq. 16) but also by the pore volume fraction and pore size.

For a small pore size ($R \to 0$) Eq. 16 recovers Hasselman's equation for thermal shock fracture of a homogeneous brittle ceramic [83].

Anisotropic polycrystalline ceramics

It has been shown that the theoretical approach used to describe the strength dependence of grain size can easily be extended to include the thermal shock fracture involving the effect of grain size and residual anisotropic stress [70, 76]. As before, fracture is assumed to originate from cracks associated with a single grain or group of grains oriented relative to neighbouring grains such that they are subjected to compressive stress acting to open the crack and surrounding grains to a tensile stress acting to close the crack. Assuming that there are N^{g} grains per unit volume favourably oriented for crack extension, the equation for a critical temperature difference (ΔT_c) was developed:

$$\Delta T_c = \left[\pi\gamma_{\text{eff}}/2(r+s)E_0\left(1-\nu^2\right)\right]^{1/2}\left[1+16\left(1-\nu^2\right)N^{\text{g}}(r+s)^3/3\right]^{1/2}\left[\alpha_{\text{av}}(1-2\nu)+\Delta\alpha/(3(1-\nu)\Phi\right]^{-1} \quad (17)$$

where r is the grain radius, α_{av} is an average linear thermal expansion of a polycrystalline anisotropic ceramic, $\Delta\alpha$ is the difference between the direction of maximum thermal expansion and the direction of minimum thermal expansion of a single grain and Φ is a constant. Although Eq. 17 was developed for an anisotropic solid, it can be applied to cubic/isotropic ceramics by taking $\Delta\alpha \to 0$ in which case Eq. 17 takes the form:

$$\Delta T_c = \left[\pi\gamma_{\text{eff}}(1-2\nu)^2/2s\alpha_{\text{av}}^2 E_0(1-\nu^2)\right]^{1/2} \left[1+16(1-\nu^2)N^{\text{g}}(r+s^3/3\right]^{1/2} \quad (18)$$

where s is the crack size and N^{g} is the number of cracks per unit volume. Again, expression (18) recovers the equation for thermal shock fracture for isotropic pore-free ceramics developed by Hasselman [83]. The role of grain size on thermal shock of a ceramic is presented in Fig. 18 which shows that, for a given flaw size, a decrease in grain size from $r = 200$ μm to $r = 75$ μm leads to an increase in thermal shock resistance a factor of 2–3.

Macrostructure–fracture toughness relationship

Despite improvements in fracture toughness, the reliability of Si_3N_4 ceramics is considerably lower compared to metals and this is considered to be a major obstacle for their wider use as structural material. One way of preventing catastrophic/brittle failure of a Si_3N_4 component is to design a structure with dense and strong Si_3N_4 layers separated by weak and/or porous layers of the same or different materials [84]. The weak interface serves to deflect the propagating crack and lower its stress intensity.

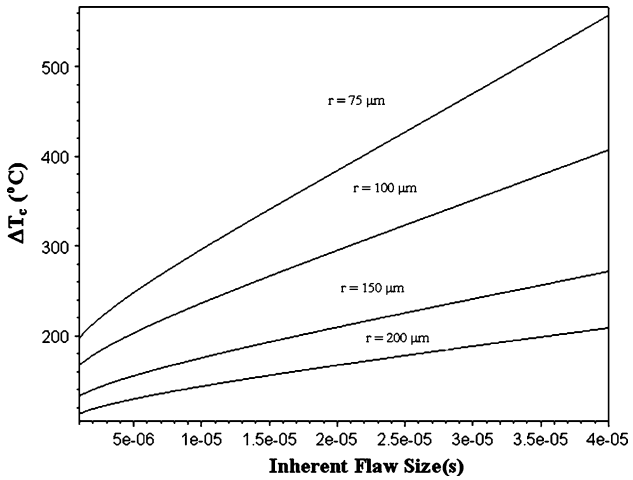

Fig. 18 Predicted change of thermal shock (ΔT_c) with inherent flaw size for a material with four different grain sizes

Laminated structures

Traditionally, the crack deflection is achieved by incorporating fibres into ceramic matrices [85, 86]. However, fabrication of the fibre-reinforced ceramics is considered to be relatively expensive and often unsuccessful in achieving required mechanical properties [87]. A far more economical way of enhancing fracture toughness of ceramics is by incorporating the weak or often porous interlayers which serve to deflect the crack as it meets the interlayer. Atkins [88] was the first who proposed this method of toughening followed by Clegg et al. [84], Zhang and Krstic [89] and Tu et al. [90]. One of the prerequisites for achieving a high apparent fracture toughness of the laminate is that the interface material must not retard the sintering process and be chemically and physically compatible with the lamina, so that they can be co-fired at an elevated temperature without any undesired reactions and delamination. This delamination, caused by internal stresses due to uneven sintering shrinkage and differences in thermal expansion coefficients, can be easily prevented by incorporating porosity in the ceramic matrix forming a porous and thus weak interlayer. Therefore, a pre-determined level of interlayer porosity required to ensure crack deflection for the situation where residual stresses were not present, has been investigated and reported by Blanks et al. [91] and Davis et al. [92]. The process of adding Si_3N_4 fibres to Si_3N_4 powder to produce porous interlayers has been reported by Ohji et al. [93]. However, one of the problems associated with a porous interlayer laminate is the difficulty of controlling the level of porosity and shape of the pores in the path of the growing interfacial crack.

In the last two decades, efforts have been directed towards the development of a plate-form laminated ceramic composite with a weak interface such as a SiC layer with a graphite interface [84, 89], which exhibits fracture toughness as high as 14 MPa $m^{1/2}$. Following this study, a number of different plate-form laminate systems were designed and fabricated including: ZrO_2/ZrO_2 [94], $Al_2O_3/LaPO_4$ [95], Si_3N_4/BN [96], Si_3N_4/Si_3N_4 and Si_3N_4/TiN [97], β-SiAlON/Si_3N_4 [98], Al_2O_3/SiC [87], Al_2O_3/ZrO_2 [99] and Al_2O_3/Al_2TiO_5 [100].

Because of their high fracture resistance and reliability, laminates have received considerable attention in the past decades. While the monolithic Si_3N_4 exhibits linear elastic behaviour until fracture (Fig. 19a), the laminated material shows a slow increase of load after the first load drop followed by further increase in load prior to fracture (Fig. 19b). This behaviour is almost identical to the fibre reinforced composites with work of fracture and apparent fracture toughness approaching those of metals. Recently, Wang et al. [101] managed to fabricate planar laminates with an apparent fracture toughness of 15.1 MPa $m^{1/2}$ by controlling the composition and structure in Si_3N_4/BN laminates. An even higher fracture toughness of 28.1 MPa $m^{1/2}$ was reported by Kovar et al. [102] who incorporated secondary reinforcement such as SiC whiskers to the BN interface. The same authors have shown that

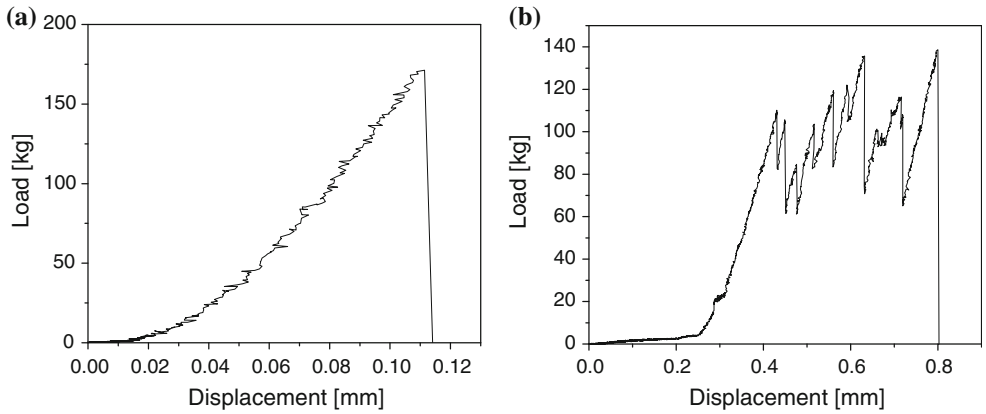

Fig. 19 Load–displacement curves for **a** monolithic Si_3N_4 and **b** laminated Si_3N_4/SiC [103]

it is also possible to achieve combination of high fracture strength (>600 MPa) and work (~8000 J/m^2) by hot-pressing Si_3N_4/BN laminates [102]. In 2005 a new type of laminated structure was designed and fabricated by Yu et al. [103]. The novelty in this design is the conversion of planar form laminates into a concentric ring structure which eliminates the direction of easy crack propagation and offers a high damage-tolerance with work of fracture of 406 kJ/m^3 and fracture toughness of over 21 MPa m$^{1/2}$.

Up until 2005, nearly all of the research in the development of Si_3N_4 laminated structures has been focused on plate-form laminates produced by tape casting and hot-pressing. Although the improvements in fracture resistance in these planar laminates were sufficient to ensure their safe use in many structural applications, delamination and easy crack propagation along the weak interface between the two layers has been the major impediment for wider use of these structures (Fig. 20) [104].

To overcome this unwanted delamination/peeling problem associated with the plate-form laminates, a concentric circular and rectangular designs have been developed and fabricated (Figs. 21, 22) in such a way that the potential delamination direction is completely eliminated [105, 106]. In addition to the absence of the direction of easy crack propagation, this new Si_3N_4/BN composite structure exhibits fracture resistance characteristics far beyond those of monolithic ceramics or planar laminates. Fracture toughness of these structures was reported to be as high as 22 MPa m$^{1/2}$ [105], fracture strength of 515 MPa [105], and work of fracture of 320 kJ/m^3 [105].

The work of fracture and apparent fracture toughness measured in these laminates are equivalent to those of unidirectional fibre reinforced composites and approach those of some metals. From a practical viewpoint, concentric ring structures do not require the employment of expensive fabrication methods such as Hot Pressing (HP) and Hot isostatic pressing (HIP) and can effectively be produced by employing traditional ceramic processing methods such as slip- and tape-castings. There are a number of variables which have to be controlled in fabricating the concentric ring structures, the most important being casting time, composition and structure of the

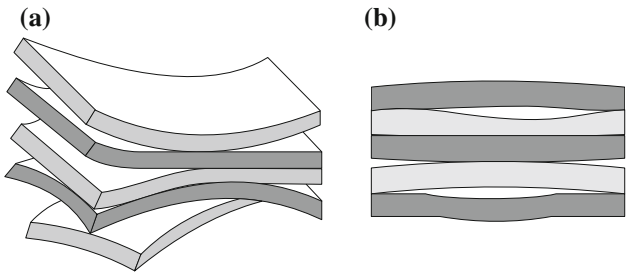

Fig. 20 **a** Peeling and **b** delamination in the plate-form laminates

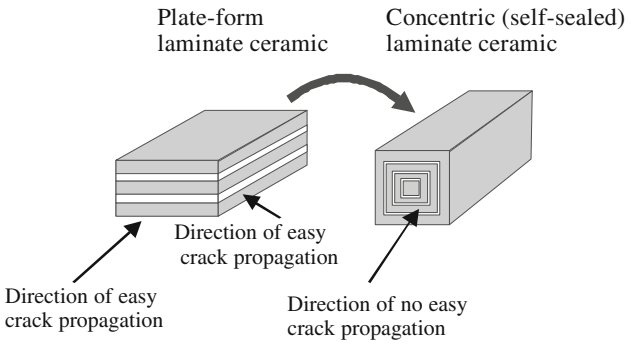

Fig. 21 New design concept-structure changes from the plate-form laminate to a concentric ring (self-sealed) structure [105]

interface and viscosity of the slurry [105]. So far, systematic studies of concentric ring structures revealed that, in addition to the composition and structure of the interface, the thickness and the number of Si_3N_4 layers control both the fracture toughness and strength of the laminate. This is shown in Fig. 23 which displays the change of apparent fracture toughness and flexural strength as a function of the number of the Si_3N_4 layers. The peak in fracture toughness and flexural strength is obtained for seven layers.

Similarly, a peak in apparent fracture toughness and strength was found to appear at some critical layer thickness which, in the case of silicon nitride laminates, is between 200 and 250 μm (Fig. 24).

A systematic study of the crack propagation and detailed examination of the interface revealed that the main toughening mechanisms in these laminates are the crack deflection at the weak interface and crack deflection and bridging within the Si_3N_4 layer by elongated β-Si_3N_4 phase. It was observed that some of these elongated particles also grew through the weak interface bridging the two silicon nitride layers. To the authors' knowledge this is the first example of the weak interface encouraging growth of elongated grains from one Si_3N_4 layer to another (Fig. 25). This appears to provide the additional strengthening and toughening to the system and makes the interface significantly stronger then otherwise it would be. This interfacial reinforcement by the elongated silicon nitride grains, bridging the two BN-based interface layers, allows creation of residual stresses which put the entire inner layers and the core of the concentric ring structure under significant compressive stress. The existence of residual stress was also recognized by Orlovskaya et al. [97], in planar Si_3N_4-based laminates, and Krstic and Krstic [106] in the concentric ring Si_3N_4 laminates who found that the level of residual stress depends on the nature/composition of the interface and Si_3N_4 layer thickness. The importance of these stresses in toughening of the concentric ring structures can best be realized by comparing the indentations made in the monolithic silicon nitride (Fig. 26a) and in the

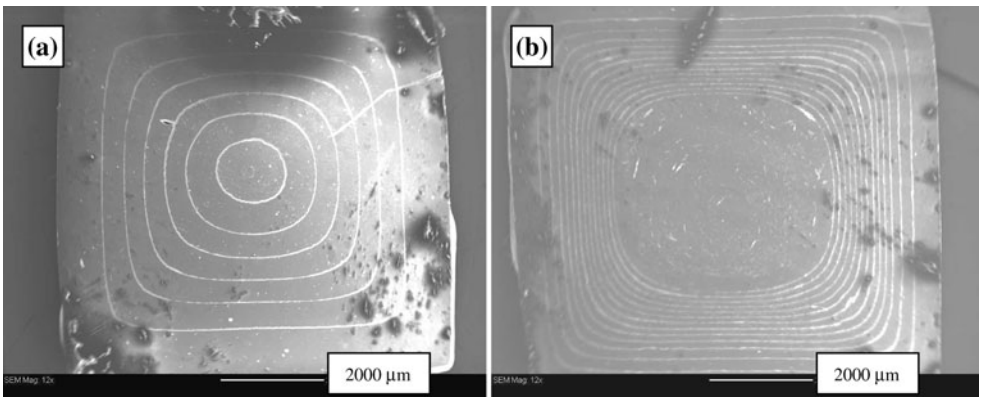

Fig. 22 SEM micrographs of cross-section of concentric Si_3N_4/BN laminated structures with **a** 6 and **b** 13 Si_3N_4 layers [105]

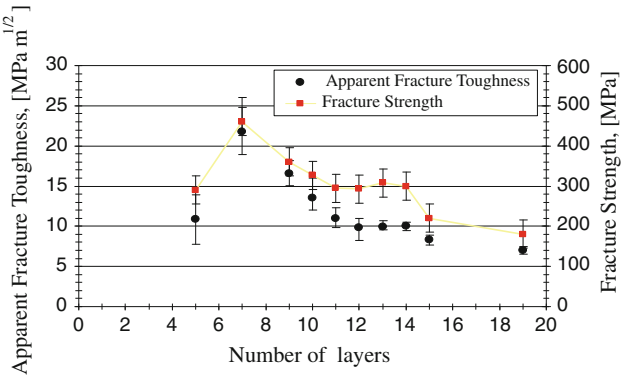

Fig. 23 Variation of apparent fracture toughness and fracture strength of concentric Si_3N_4/BN laminated structure with the number of Si_3N_4 layers [104]

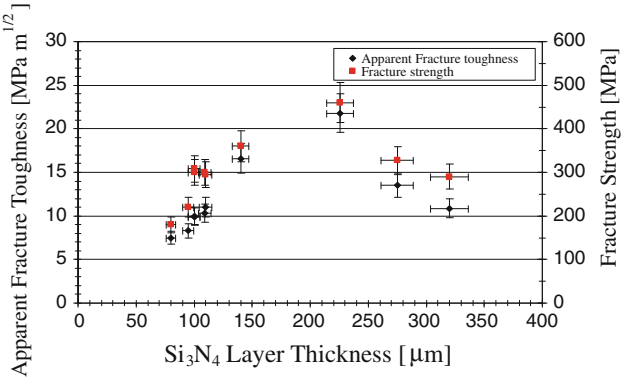

Fig. 24 Effect of Si_3N_4 layers thickness on fracture toughness and strength of concentric Si_3N_4/BN laminated structure [104]

core of the concentric ring structure applying the same indentation load of 30 kg. While cracks larger than 300 µm were observed in unstressed monolithic Si_3N_4, no cracks were detected in laminated Si_3N_4 (Fig. 26b) [106]. Also, the

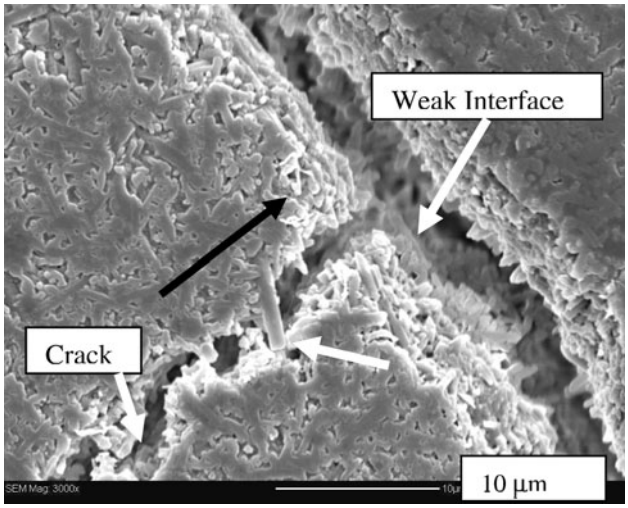

Fig. 25 SEM image of chemically etched Si_3N_4/BN laminated structure showing crack propagation and its deflection and arrest at the week interface, and elongated β-Si_3N_4 bridging grain pull out at the surface of the crack [104]

indentation diagonal is approximately 100% larger in monolithic silicon nitride compared to its laminated counterpart. This demonstrates clearly that the residual stress puts the inner volume of the concentric ring structure under compression inhibiting crack propagation and providing the additional degree of toughening. The level of residual stress was found to also depend on the composition of the "weak" interfacial layer. For example, laminates with interfacial layers with BN and Si_3N_4 exhibit a lower degree of toughening compared to layers produced with BN and Al_2O_3. The toughening mechanism operating in concentric Si_3N_4/BN laminated composites is shown in Fig. 25. The direction of the crack propagation (pointed by the black arrow), and the bridging grain pull out at the surface of the crack, within the Si_3N_4 layers (the white arrow), and the crack deflection which was arrested at the weak interface is clearly shown in Fig. 25.

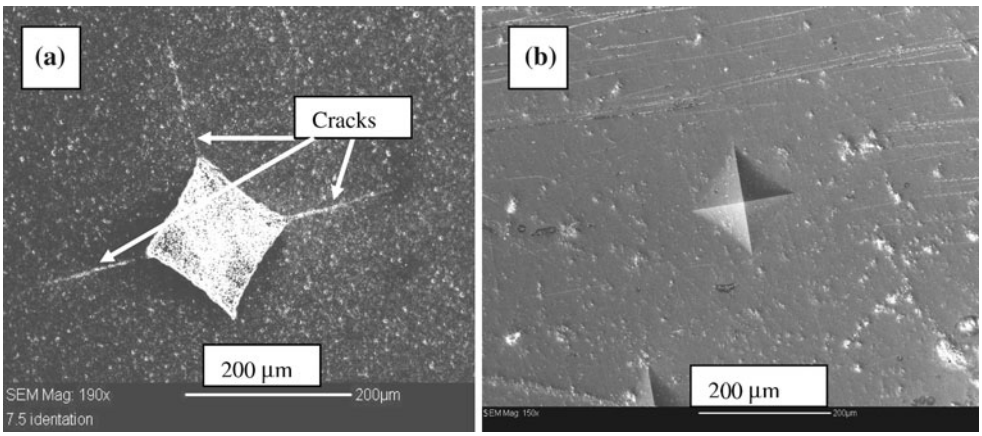

Fig. 26 Comparison of crack lengths developed under the same load of 30 kg in **a** unstressed monolithic Si_3N_4 ($K_{IC} = 7.98$ MPa $m^{1/2}$) and **b** stressed Si_3N_4/BN-based laminated structures ($K_{IC} = 18.87$ MPa $m^{1/2}$) [106]

Summary

Over the last decades, significant progress has been made in the development of a new generation of silicon nitride ceramics with mechanical properties far exceeding those of classical counterparts. Specifically, there are three general areas where the effort was focused.

First is the area of microstructure development where it was possible to grow β-Si_3N_4 grains with an almost perfect circular cross-section and an aspect ratio that encouraged crack pull-out and crack bridging, both of which are identified as the most powerful mechanisms of toughening and strengthening. This, combined with compositional refinement of the interface, has led to a major enhancement of the fracture toughness of monolithic silicon nitride ceramics to a level not found in the past.

The second major development lies in the design and fabrication of a concentric ring structure consisting of dense homogeneous silicon nitride layers and a weak, partially porous interface that encourages crack deflection and toughening. The advantage of this type of structure is that it eliminates the direction of easy crack propagation which was the major problem with classical planar laminates. An enormous increase in fracture toughness was achieved with measured apparent fracture toughness of over 21 MPa $m^{1/2}$. This high toughness, which approaches that of aluminium alloys, has not been found in other ceramics and opens the avenue for the use of silicon nitride ceramics in applications previously reserved only for metals.

The third area of advancement is in the theoretical understanding of fracture of ceramics and its implications for the future development of a strong and reliable ceramic. The theory developed describes a unified approach to fracture, one that embodies the effect of key microstructural features on strength. While in the past the effects of crack size, grain size and residual stresses were treated in isolation, the new approach unifies these effects into a single equation. For example, it has been shown that the full characterization of a porous ceramics involves not only the knowledge of pore volume fraction but also the pore size and the crack size. The theory shows that the presence of larger number of smaller size pores is much more beneficial for an achieved higher strength than the smaller size of larger pores. Similarly it has been shown that the strength of polycrystalline anisotropic ceramic, such as silicon nitride, is controlled not only by the grain size but also by the inherent flaw size and residual anisotropic stress. An important practical implication of this theoretical finding is that the fabrication of high strength polycrystalline anisotropic ceramics may be achieved not only by reducing grain size but also by decreasing the inherent flaw size (also called the processing flaws). A decrease in grain size to a submicron and nanosize will not lead to an increase in strength unless the flaw size is also kept small.

References

1. Poper P (1994) Key Eng Mater 89–91:719
2. Berroth K, Prescher T, Schubert J (2005) 3rd DRACHE-seminar casting techniques, Lahnstein, Germany, May 9–11, 2003
3. Taffner U, Carle V, Schafer U, Predel F, Petzow G (1991) Prakt Met 28:592
4. Mazzocchi M, Bellosi A (2008) J Mater Sci Mater Med 19:2881
5. Mazzocchi M, Gardini D, Traverso PL, Faga MG, Bellosi A (2008) J Mater Sci Mater Med 19:2889
6. Neumann A, Reske T, Held M, Jahnke K, Ragoß C, Maier HR (2004) J Mater Sci Mater Med 15:1135
7. Jack KH (1976) J Mater Sci 11:1135. doi:10.1007/BF00553123
8. Weiss J (1981) Ann Rev Mater Sci 11:381
9. Hampshire S (2007) J Achiev Mater Manuf Eng 24(1):43
10. Wild S, Grieveson P, Jack KH (1972) Spec Ceram 5(271–284):385
11. Grieveson P, Jack KH, Wild S (1968) Spec Ceram 4:237
12. Henderson CMB, Taylor D (1975) Trans J Br Ceram Soc 74:49

13. Tanaka H (1991) In: Somiya S, Inomata Y (eds) Silicon carbide ceramics-1, fundamental and solid reaction. Elsevier, New York, NY, p 213
14. Greskovich C, Rosolowski JH (1975) J Am Ceram Soc 59(7–8):336
15. Kingery WD (1959) J Appl Phys (a) 30(3):301
16. Barsoum M (1977) Fundamentals of ceramics. McGraw-Hill, New York
17. Coble RL (1958) J Am Ceram Soc 41:55
18. Krstic Z, Krstic VD (2002) Diffusion coefficient of Si_3N_4 during solution-reprecipitation stage of liquid phase sintering, unpublished work
19. Thummler F (1980) Mater Sci Res 13:247
20. Hampshire S, Jack KH (1975) Spec Ceram 6:37
21. Suematsu H, Mitomo M, Mitchel TE, Petrovic JJ, Fukunaga O, Ohashi N (1997) J Am Ceram Soc 80(3):615
22. Natansohn S, Sarin VK (1988) In: Hausner H, Messing G, Horano GL (eds) Ceramic powder processes science. Dtch. Keram. Ges., Cologne, p 433
23. Lifshitz IM, Slyozov VV (1961) J Phys Chem Solids 19:35
24. Wagner C (1961) Z Elektrochem 65:581
25. Tien TY (1995) In: Alper AM (ed) Study of silicon nitride ceramics, phase diagrams in advanced ceramics. Academic Press, San Diego, p 127
26. Lai KR, Tien TY (1991) Bimon. Rep. ceramic technology for advanced heat engine project. Oak Ridge National Laboratory, Oak Ridge, TN
27. Krstic VD, Bellosi A, Bucciotti F, Krstic Z (2011) Microstructure and mechanical properties of pressureless sintered and HIP-ed silicon-nitride ceramics, unpublished work
28. Becher PF, Painter S, Shibatam N, Waters SB, Lin H-T (2008) J Am Ceram Soc 91(7):2328
29. Painter JS, Averill FW, Becher PF, Shibata N, Van Benthem K, Pennycook SJ (2008) Phys Rev B 78:214201
30. Shibata N, Pennycook SJ, Gosne TR, Painter GS, Shelton WA, Becher PF (2004) Nature 428:730
31. Averill FW, Painter GS (2008) Phys Rev B 77:155109
32. Shibata N, Painter GS, Becher PF, Pennycook SJ (2006) Appl Phys Lett 89:051908
33. Deeley GG, Herbert JM, Moore NC (1961) Powder Metall 8:145
34. Tsuge A, Nishida K, Komatsu M (1975) J Am Ceram Soc 58:323
35. Jack KH (1979) 4th CIMTEC, energy and ceramics, St. Vincent, Italy
36. Gauckler LJ, Boskovic S, Petzow G, Tien TY (1977) In: Riley FL (ed) Nitrogen ceramics. Nordhoff, Leyden, p 405
37. Gauckler LJ, Petzow G (1977) In: Riley FL (ed) Nitrogen ceramics. NATO Advanced Study Institute Series. Nordhoff, Leyden, p 41
38. Oda I, Kaneno M, Yamamoto N (1977) In: Riley FL (ed) Nitrogen ceramics. Nordhoff, Leyden, p 359
39. Rice RW, McDonough WJ (1975) J Am Ceram Soc 58:264
40. Wallace JS, Kelly JF (1994) Key Eng Mater 89–91:501
41. Park D-S, Lee S-Y, Kim H-D, Yoo B-J, Kim B-A (1998) J Am Ceram Soc 81(7):1876
42. Nishimura T, Mitomo M (1996) J Mater Res 12:203
43. Kargin YuA, Lysenkov AS, Ivicheva SN, Zakharov AI, Popova NA, Solntsev KA (2010) Inorg Mater 46(7):799
44. Furuya K, Munakata F, Matsuo K, Akimune Y, Ye J, Okada A (2002) J Therm Anal Calorim 69:873
45. Hoffmann MJ, Geyer A, Oberacker R (1999) J Eur Ceram Soc 19:2359
46. Bressiani JC, Genova LA (2006) Adv Sci Technol 45:1717
47. Prochaska S, Greskovich C (1978) Effects of some impurities of sintering Si_3N_4. General Electric Report, vol 204, p 78
48. Becher PF, Hwang S-L, Hsueh C-H (1995) Using microstructure to attack the brittle nature of silicon nitride ceramics. MRS Bulletin, February 23–27
49. Krstic VD (2000) In: Song J, Yin R (eds) Proceedings of international conference on engineering and technological science, vol 1. Chinese Academy of Engineering, Beijing, China, p 83
50. Drew P, Lewis MH (1974) J Mater Sci 9:261. doi:10.1007/BF00550950
51. Lange FF (1979) J Am Ceram Soc 62(7–8):428
52. Woetting G, Kanka B, Ziegler G (1986) In: Hampshire S (ed) Non-oxide technical and engineering ceramics. Elsevier, London, p 83
53. Tani E, Umebayashi K, Kishi K, Kobayashi K, Nishijama M (1985) J Mater Sci Lett 4:1454
54. Pyzik AJ, Hart AM (1995) In: Alper AM (ed) Phase diagrams in advanced ceramics. Academic Press, San Diego, p 199
55. Mitomo M, Tsutsumi M, Tanaka H, Uenosono S, Saito F (1990) J Am Ceram Soc 73(8):2441
56. Neil JT, Bandyopadhyay G, Sordelet D, Mahoney M (1989) Annu Meet Auton Technol Dev Contam Coord
57. Krstic Z, Krstic VD (2003) Mater Sci Forum 413:129
58. Krstic Z, Yu Z, Krstic VD (2007) J Mater Sci 42:5431. doi:10.1007/s10853-006-0826-9
59. Griffith AA (1921) Philos Trans R Soc Lond A 221:163
60. Griffith AA (1924) Proceedings of the 1st international congress applied mechanics, p 55
61. Faber KT, Evans AG (1983) Acta Metall 31(4):577
62. Mulla MA, Krstic VD (1994) Acta Metal Mater 42(1):303
63. Becher PF, Shibata N, Painter GS, Averill F, Van Benthem K, Lin H-T, Waters SB (2010) J Am Ceram Soc 93(2):570
64. Fett T, Oberacker R, Hoffman M, Schneider GA, Becher P, Kruzic JJ (2011) J Am Ceram Soc 84(6):1884
65. Krstic VD (1985) Acta Metall 33(3):521
66. Knudsen FP (1962) J Am Ceram Soc 45:94
67. Rice RW (1984) J Mater Sci 19:895. doi:10.1007/BF00540460
68. Krstic VD (1985) Acta Metall 33:521
69. Krstic V, Erb U, Palumbo G (1993) Scripta Metall Mater 29:1501
70. Krstic VD (1988) J Mater Sci 23:259. doi:10.1007/BF01174063
71. Krstic VD (1983) J Am Ceram Soc 66(10):726
72. Krstic VD, Vlajic MD (1983) Acta Metall 31:139
73. Krstic VD (1984) J Am Ceram Soc 67(9):589
74. Krstic VD, Komac M, Vlajic MD (1984) J Mater Sci 19:4119. doi:10.1007/BF00980779
75. Wang G, Krstic VD (1998) Philos Mag A 78(5):1125
76. Krstic VD (2006) Theor Appl Fract Mech 45:212
77. Krstic VD, Erickson WH (1987) J Mater Sci 22:2881. doi:10.1007/BF01086485
78. Nieman GW, Weertman JR, Siegel RW (1991) J Mater Res 6:1012
79. Zugic R, Szpunar B, Krstic VD, Erb U (1997) Philos Mag 75(4):1041
80. Krstic Z, Krstic VD (2002) Effect of porosity on fracture strength of Si_3N_4 sintered with Y_2O_3 and Al_2O_3, unpublished work
81. Selsing J (1961) J Am Ceram Soc 44:419
82. Krel A, Blank P (1996) J Eur Ceram Soc 16:1189
83. Hasselman DPH (1969) J Am Ceram Soc 52:600
84. Clegg WJ, Kendall K, Alford NM, Birchall D, Button TW (1990) Nature 347:455
85. Kovar D, King BH, Trice RW, Halloran JW (1997) J Am Ceram Soc 80:2471
86. Koh Y-H, Kim H-W, Kim H-E (2002) J Am Ceram Soc 85:2840
87. She J, Inoe T, Ueno K (2000) J Eur Ceram Soc 20:1771
88. Atkins AG (1974) Nature 252:116
89. Zhang L, Krstic VD (1995) Theor Appl Fract Mech 24:13
90. Tu W-C, Lange FF, Evans AG (1996) J Am Ceram Soc 79:424
91. Blanks KS, Kristofferson A, Carlstorm E, Clegg WJ (1998) J Eur Ceram Soc 18:1945

92. Davis JB, Kristofferson A, Carlstorm E, Clegg WJ (2000) J Am Ceram Soc 83:2369
93. Ohji T, Shigegaki Y, Miyajima T, Kanzaki S (1997) J Am Ceram Soc 80:991
94. Sanchez-Herencia AJ, Pascual C, He J, Lange FF (1999) J Am Ceram Soc 82:1512
95. Mawdsley J, Kover D, Halloran JW (2000) J Am Ceram Soc 83:802
96. Liu H, Hsu SM (1996) J Am Ceram Soc 79:2452
97. Orlovskaya N, Kuebler J, Subbotin V, Lugovy M (2005) J Mater Sci 40:5443. doi:10.1007/s10853-005-1918-7
98. Shigegaki Y, Brito ME, Hirao K, Toriyama M, Kanzaki S (1997) J Am Ceram Soc 80:2624
99. Plucknett KP, Caceres CH, Hughers C, Wilkinson DS (1994) J Am Ceram Soc 77:2145
100. Russo CJ, Harmer MP, Chan MH, Miller GA (1992) J Am Ceram Soc 75:3396
101. Wang C, Huang Y, Zan Q, Zou L, Cai S (2002) J Am Ceram Soc 85:2457
102. Kovar D, Thouless MD, Halloran JW (1998) J Am Ceram Soc 81:1004
103. Yu Z, Krstic Z, Krstic VD (2005) Key Eng Mater 280–283:1873
104. Krstic Z, Krstic VD (2009) J Eur Ceram Soc 29:1825
105. Krstic Z, Krstic VD (2008) J Eur Ceram Soc 28:1723
106. Krstic Z, Krstic VD (2011) J Eur Ceram Soc 31:1841